Ecological Modelling 524 (2027) 111932

Contents lists available at ScienceDirect

Ecological Modelling

journal homepage: www.elsevier.com/locate/ecolmodel

Incorporating crowding into integrated integral population models

Iván Romero-García [a,b], Eugenio Larios [c,d], Edgar J. González [a,*]

[a] Departamento de Ecología y Recursos Naturales, Facultad de Ciencias, Universidad Nacional Autónoma de México, Circuito Exterior s/n, Ciudad Universitaria, Coyoacán, 04510, Mexico City, Mexico
[b] Posgrado en Ciencias Biológicas, Unidad de Posgrado, Edificio D, 1° Piso, Circuito de Posgrados, Ciudad Universitaria, Coyoacán, 04510, Mexico City, Mexico
[c] Programa Educativo Licenciatura en Ecología, Universidad Estatal de Sonora, Ley Federal del Trabajo s/n, Apolo, 83100, Hermosillo, Sonora, Mexico
[d] Ecología para la Conservación del Gran Desierto, A.C., Roberto Romero 63, Jesús García, 83140, Hermosillo, Sonora, Mexico

ARTICLE INFO

Keywords:
Crowding effect
Integral projection model
Integrated population models
Population dynamics
Neighborhood
Spatial structure

ABSTRACT

Intraspecific interactions influence the dynamics of individuals and can extend to the population level. In plants, these interactions are determined by individuals' relative positions, and because their spatial distribution is heterogeneous in nature, individuals do not experience the same degree of interspecific and intraspecific interactions, with the latter generally being more intense due to competition for shared resources. In this study, we developed a Spatially Structured Integrated Integral Population Model (SSIIPM) that incorporates the spatial relationships between conspecific individuals as an approximation of intraspecific interactions, evaluating their effects on vital rates and, ultimately, on population dynamics. The model includes individual size and crowding effect as state variables and integrates population-level data to improve estimates of population size, structure, and establishment probability. We illustrate the SSIIPM using 23 years of demographic data from an acuña cactus population at Organ Pipe Cactus National Monument, Arizona, USA. Individual size explained most of the variation in vital rates. Crowding reduced individual growth, had no detectable effect on survival or fecundity, and showed a positive but uncertain association with reproduction probability. The SSIIPM successfully captured the observed population decline over time, owing to the integration of population-level data. From these results, we can state that incorporating crowding as a state variable in a population dynamics model allows identifying the differential effects that neighbors have on the vital rates of a focus individual and, as an extension, on the population.

1. Introduction

The spatial arrangement of environmental factors influences plant population dynamics, a fact long recognized by ecologists (Dunning et al., 1995; Hutchings et al., 2003; Jiménez-Guzmán et al., 2024; Pacala, 1987). It affects individual survival and reproduction, shaping population dynamics (Crone, 2016). Models of population dynamics have incorporated spatially varying abiotic factors, such as climate (McIntosh et al., 2020; Merow, Latimer, et al., 2014; Sanczuk et al., 2023), radiation (Scanga, 2014), soil nutrients (Dahlgren and Ehrlén, 2009; Hutchings et al., 2003), and topography (Hamrick and Lee, 1987). While these influences are well established, less attention has been given to biotic spatial variation, including the distribution and interactions of individuals, which also drive population dynamics (Adler, et al., 2018a).

Plants interact more with nearby plants than those farther away (Barber et al., 2022; Tyler and D' Antonio, 1995). The irregular spatial distribution of individuals means some plants experience more interactions than others (Dunning et al., 1995; Zhang et al., 2022). Intraspecific competition is generally stronger than interspecific competition, mainly due to niche differentiation among species, which in turn promotes coexistence in plant communities (Adler et al., 2018a). Consequently, conspecific interactions likely influence vital rates more than heterospecific ones, with a greater effect on population dynamics. Interaction effects can also be size-dependent (Jia and Zhang, 2024; Lin et al., 2012; Schwinning and Weiner, 1998) and shift from positive (facilitation) to negative (competition) throughout an individual's life cycle (Aranda-Pineda et al., 2021; Callaway and Walker, 1997). For instance, mature plants may nurse saplings, but as saplings mature, this interaction can turn competitive (Armas and Pugnaire, 2009; Miriti, 2006). Thus, plant interactions are dynamic.

Given the dynamic nature of plant interactions and their effects on

* Corresponding author at: Circuito Exterior s/n, Ciudad Universitaria, Coyoacán, 04510, Mexico City, Mexico.
E-mail address: edgarjgonzalez@ciencias.unam.mx (E.J. González).

https://doi.org/10.1016/j.ecolmodel.2026.111932

0304-3800/© 2026 The Authors. Published by Elsevier B.V. This is an open access article under the CC BY license (http://creativecommons.org/licenses/by/4.0/).

vital rates, understanding their impact on population dynamics is crucial. These dynamics can be summarized by changes in population structure, defined as the distribution of state variables at a given time (Metz, 2008). Intrinsic state variables, such as sex, age, or size (Ellner et al., 2016), are commonly used in population dynamics models, assuming individuals with similar values of their state variables contribute similarly to population dynamics (Ellner et al., 2016; Rees et al., 2014). Populations can also be structured by extrinsic factors, such as microenvironmental conditions (Sanczuk et al., 2023). However, a third type of state variables are those that reflect the interactions between pairs of individuals, which in this sense are neither intrinsic nor extrinsic.

A way to introduce plant interactions into population dynamics models is through the neighborhood or crowding effect (w), which considers the distance between a focal individual and every neighbor, along with their size, to predict the focal individual's vital rates (Pacala, 1987; Hara, 1988). Because vital rates respond differently to crowding (Lyu and Alexander, 2023), the spatial distribution of individuals reflects the response of vital rates to crowding and other environmental factors. While w has been viewed as a population-level constant (Preuss et al., 2009; Vanoverbeke, 2008), so that all individuals experience the same degree of crowding at a given time, or as a function of the focal individual's size (Adler et al., 2010, 2012; Adler et al., 2018b; Teller et al., 2016), assuming these types of relations in plants is an oversimplification because focal individuals of the same size can occupy neighborhoods with very different crowding levels (Tamura et al., 2019).

The varying effects of state variables on vital rates, including w, highlights the need for models to capture both individual-level variability and spatial interactions within populations. Structured population dynamic models are particularly effective, as they incorporate variation in traits like size or age alongside environmental drivers, offering a more accurate representation of population processes. Integral Projection Models (IPMs), which have become increasingly relevant in population ecology over the past decades (Doak et al., 2021), model changes in population structure over time using a continuous state variable (z). IPMs link vital rates to z via regression models and integrate them into a kernel to project population dynamics (Ellner et al., 2016; Merow, Latimer, et al., 2014; Rees et al., 2014). Beyond state variables, IPMs can include environmental drivers, meaning individual demographic fates are influenced by both intrinsic and extrinsic factors. However, interactions between individuals are rarely incorporated into IPMs (Merow, Dahlgren, et al., 2014) nonetheless, examples exist.

The crowding effect has been included in IPMs as a state variable, affecting the survival and growth of individuals (Adler et al., 2010, 2012; Adler et al., 2018b; Teller et al., 2016). In these IPMs these vital rates depend on both the size of the individuals and the crowding they experience. These models make certain assumptions, such as that the distance between individuals is a discrete variable and that reproduction does not depend on the crowding experienced. Additionally, even though each individual has a different response to the crowding they experience, and this response changes through time, it is considered as a variable whose values depend strictly on the size of the focal individual and not on its position, i.e., it is not included as a variable that changes due to changes in the focal individual and its neighbors' positions and presence.

The population structure for a given state variable is an emergent property at the population level. To accurately project population structures over time, an IPM must describe them correctly during the study period. Previous work highlighted challenges in predicting population-level attributes from individual-level data (Ghosh et al., 2012). Portillo-Tzompa et al. (2023) addressed this by developing a Bayesian Integrated Integral Population Model (IIPM), which combines the individual-level approximation of a traditional IPM with the inverse IPM (InvIPM) approach of González et al. (2016). The IIPM integrates individual and population data, estimating posterior distributions for vital rate parameters, initial population structure and size (Portillo-Tzompa et al., 2023). By incorporating both individual size and crowding as state variables, an IPM can fit observed joint size and crowding effect structures.

The aim of this study was to develop a methodology for analyzing the dynamics of a population structured by the crowding effect as a proxy to how intraspecific interactions affect said dynamics. We present an IIPM in which the population is structured by an intrinsic variable, individual size in our case, and the crowding effect. We exemplify this model with a 23-year long survey of an endangered globose cactus, *Echinomastus erectocentrus* var. *acunensis*, inhabiting the Organ Pipe Cactus National Monument (OPCNM), Arizona, USA.

2. Methods

2.1. IPM theory

IPMs consist of a function $K(z', z)$, called the *kernel*, which describes the dynamics of an average individual according to its state variable. This function allows approximating the population structure, $n_{t+1}(z)$. At time t the population structure is $n_t(z)$, which, iterated with K, approximates the population structure at time $t+1$, through

$$n_{t+1}(z') = \int K(z', z) \cdot n_t(z) dz, \tag{1}$$

where z' is the state variable at time $t+1$ (Ellner et al., 2016; Merow, Dahlgren, et al., 2014; Rees et al., 2014). The integral spans the interval $[L_z, U_z]$, corresponding to the smallest and largest observed values of the state variable. To approximate the integral numerically, this interval is divided into N_i bins. The population size at time $t+1$ is

$$N_{t+1} = \int n_{t+1}(z') dz'. \tag{2}$$

The kernel in Eq. (1) consists of the following vital rate functions: 1) the survival function, $s(z)$, describing the probability of an individual with state z at time t surviving to $t+1$; 2) the growth function, $G(z', z)$, describing the probability of transitioning from z at t to z' at $t+1$; 3) the reproduction probability, $p(z)$, for an individual with state z; 4) the mean number of newborns produced by an individual with state z, $f(z)$; and 5) the newborn state distribution, given by $C(z', z)$ if linked to a parent or $c(z')$ otherwise. Thus, the kernel can be described as

$$K(z', z) = s(z) \cdot G(z', z) + p(z) \cdot f(z) \cdot c(z'). \tag{3}$$

A traditional IPM uses generalized linear models (GLMs) to fit the vital rates that integrate the kernel of the IPM, i.e.,

$$s(z) = logistic\left(\beta_{0,s} + \beta_{1,s} \cdot z\right), \tag{4}$$

$$G(z', z) \sim Normal\left(\beta_{0,G} + \beta_{1,G} \cdot z, \sigma_G\right),$$

$$p(z) = logistic\left(\beta_{0,p} + \beta_{1,p} \cdot z\right),$$

$$f(z) = exp\left(\beta_{0,f} + \beta_{1,f} \cdot z\right) + 1,$$

$$c(z') \sim Normal(\mu_c, \sigma_c).$$

The likelihood of the entire IPM is the sum of the likelihoods associated with the vital rates, $l(\boldsymbol{s} \mid \beta_s)$, $l(\boldsymbol{G} \mid \beta_G, \sigma_G)$, $l(\boldsymbol{p} \mid \beta_p)$, $l(\boldsymbol{f} \mid \beta_f, \sigma_f)$ and $l(\boldsymbol{c} \mid \mu_c, \sigma_c)$, where the terms on the left side of $\mid$ are the vital rate data, and β are the parameters associated to the mean of the distribution and σ is the dispersion parameter of said distribution.

2.2. Development of an IPM that takes crowding into account

In the present work we consider the crowding effect as a dual variable that influences the IPM's kernel, and in the context of this study we

refer to such IPM as a Spatially Structured Integral Projection Model (SSIPM). An SSIPM that considers w and an intrinsic state variable has a kernel of the form

$$K(z',z,w',w) = s(z,w)\cdot G(z',z,w',w) + p(z,w)\cdot f(z,w)\cdot c(z',w') \quad (5)$$

In Eq. (5) the survival, growth, probability of reproduction and the number of newborns produced do not only depend on the state variable z of the individuals, but also of the w the individual experiences. It is also important to mention that in this model we are only considering the intraspecific interactions, positive and negative, but not of interspecific ones.

To estimate the crowding effect experienced by an individual i we used the *interaction kernel* (W),

$$W(u_i,u_j) = exp\left(\left(-D(u_i,u_j)/\eta\right)^{\psi}\right), \quad (6)$$

where $\boldsymbol{u}_i$ and $\boldsymbol{u}_j$ are the coordinates of the focal individual i and the neighbor j, respectively, D is the Euclidean distance between the individuals i and j, η determines the dispersion of the interaction kernel, and ψ the kurtosis of the interaction kernel. To avoid the edge effect (Baddeley et al., 2015; Haefner et al., 1991), these distances were corrected using a torus (see Supplementary Material I). With W, the crowding effect experienced by a focal individual i is

$$w_i = \sum\nolimits_j z_j\cdot W(u_i,u_j), \quad (7)$$

where, z_j is the size of the neighbor j. Thus, a larger neighbor contributes more to the w experienced by the focal individual than a smaller one. The units of w are log(mm)·e^{cm}. Units will not be referenced further to simplify the main text.

In our model we assume that w impacts, and it is common to, all vital rates. Therefore, the vital rates that define the SSIPM kernel are

$$\begin{aligned} &s(z,w) = logistic\left(\beta_{0,s} + \beta_{1,s}\cdot z + \beta_{2,s}\cdot w\right),\\ &G(z',z,w',w) = G(z',z)\cdot G(w',w),\\ &p(z,w) = logistic\left(\beta_{0,p} + \beta_{1,p}\cdot z + \beta_{2,p}\cdot w\right),\\ &f(z,w) = exp\left(\beta_{0,f} + \beta_{1,f}\cdot z + \beta_{2,f}\cdot w\right), and\\ &c(z',w') = c(z')\cdot c(w') \end{aligned} \quad (8)$$

where

$$\begin{aligned} &G(z',z) \sim Normal\left(\beta_{0,G,z} + \beta_{1,G,z}\cdot z + \beta_{2,G,z}\cdot w, \sigma_{Gz}\right),\\ &G(w',w) \sim Normal\left(\beta_{0,G,w} + \beta_{1,G,w}\cdot z + \beta_{2,G,w}\cdot w, \sigma_{Gw}\right),\\ &c(z') \sim Normal\left(\mu_{c,z}, \sigma_{cz}\right),\\ &c(w') \sim Normal\left(\mu_{c,w}, \sigma_{cw}\right). \end{aligned}$$

The parameters β_2 determine whether crowding acts as competition ($\beta_2 < 0$) or facilitation ($\beta_2 > 0$) on the vital rate. Survival and reproduction probabilities follow a Bernoulli distribution, and the number of descendants follows a negative binomial distribution. The rest of the models followed the probability distributions described in equations 8. To avoid the unintentional eviction of individuals described by Williams et al. (2012), we redistributed the area under the curve to ensure it integrates to one, which is a solution they recommended.

After modifying the equations describing the vital rates, the SSIPM can be formulated as

$$n_{t+1}(z',w') = \int_z\int_w K(z',z,w',w)\cdot n_t(z,w)dzdw. \quad (9)$$

Because the value of w is determined by the parameters η and ψ, the model needs to estimate jointly all its parameters, and its likelihood is the sum of $l(\boldsymbol{s} \mid \boldsymbol{\beta}_s, \eta, \psi)$, $l(\boldsymbol{G} \mid [\mu_{G,z}, \mu_{G,w}], \boldsymbol{\Sigma}_G, \eta, \psi)$, $l(\boldsymbol{p} \mid \boldsymbol{\beta}_p, \eta, \psi)$, $l(\boldsymbol{f} \mid \boldsymbol{\beta}_f, \sigma_f, \eta, \psi)$ and $l(\boldsymbol{c} \mid [\mu_{c,z}, \mu_{c,w}], \boldsymbol{\Sigma}_c, \eta, \psi)$.

So far, we have described a spatially structured IPM that relies solely on individual-level data to estimate parameters. This model omits the probability of establishment for new individuals due to the lack of information, leading to overestimated population sizes. To address this, we developed a Spatially Structured IIPM (SSIIPM), incorporating population-level data such as structure and size to infer the probability of establishment. This approach enables parameter estimation for kernels lacking direct information.

2.3. Taking population data into account: SSIIPM

The SSIIPM builds on the SSIPM described earlier and the IIPM developed by Portillo-Tzompa et al. (2023). It employs a Bayesian framework to integrate individual and population data, enabling the estimation of posterior distributions for vital rate parameters in equations 8. Additionally, the SSIIPM estimates: (1) intercepts $\boldsymbol{\alpha}_0$, which, after applying the softmax function (Gu et al., 2023; Ren and Wang, 2023), correspond to the discretized initial population distribution $\boldsymbol{d}_0$; and (2) the initial population size N_0, yielding an initial population structure $n_0(z, w) = N_0\cdot d_0(z, w)$.

The SSIIPM also estimates parameters for kernels where data is absent, such as the establishment probability (q), which is informed by population-level data. Since information on q varying with z'and w' is unavailable, q is assumed constant across all newborns, irrespective of their size or crowding effect. Consequently, Eq. (5) is modified as:

$$K(z',z,w',w) = s(z,w)\cdot G(z',z,w',w) + p(z,w)\cdot f(z,w)\cdot q\cdot c(z',w'). \quad (10)$$

To evaluate the goodness of fit for estimated population sizes and structures over time, we modeled N_t using a negative binomial distribution with a mean derived from $N_{t+1} = \int\int n_{t+1}(z', w')dz'dw'$, and a multinomial distribution to describe the discretized $n_t(z', w')$ using relative frequencies from Eq. (9). Since this model incorporates individual- and population-level data, its likelihood combines the vital rate likelihoods $l(\boldsymbol{s} \mid \boldsymbol{\beta}_s, \eta, \psi)$, $l(\boldsymbol{G} \mid [\mu_{G,z}, \mu_{G,w}], \boldsymbol{\Sigma}_G, \eta, \psi)$, $l(\boldsymbol{p} \mid \boldsymbol{\beta}_p, \eta, \psi)$, $l(\boldsymbol{f} \mid \boldsymbol{\beta}_f, \sigma_f, \eta, \psi)$ and $l(\boldsymbol{c} \mid [\mu_{c,z}, \mu_{c,w}], \boldsymbol{\Sigma}_c, \eta, \psi)$, with the likelihood of population structures $l(\boldsymbol{n}_t \mid \boldsymbol{\alpha}_0, \boldsymbol{\theta})$ and sizes $l(N_t \mid N_0, \sigma_0, \boldsymbol{\theta})$, where $\boldsymbol{\theta} = \{\boldsymbol{\beta}_s, [\mu_{G,z}, \mu_{G,w}], \boldsymbol{\Sigma}_G, \boldsymbol{\beta}_p, \boldsymbol{\beta}_f, \sigma_f, [\mu_{c,z}, \mu_{c,w}], \boldsymbol{\Sigma}_c, \eta, \psi\}$.

2.4. Study case

The acuña cactus (*Echinomastus erectocentrus* var. *acunensis*) is a globose, single-stemmed species reaching up to 40 cm in height and 10 cm in width. It is primarily found atop granite knolls in the Acuña basin, often in areas devoid of vegetation. This cactus reproduces annually, producing 7–8 flowers on the apical meristem from mid-March to early April, with fruits ripening in May. Its flowers are pollinated by native bees of the genera *Megachile* and *Diadasia* (Johnson, 1992), and its fruits contain about 100 seeds dispersed by rodents and ants via endozoochory (Larios, unpublished data). Listed as Endangered under the Endangered Species Act since 2013 (U.S. Fish and Wildlife Service, 2013), its restricted distribution (seven known sites, each <45 km^2) and threats like poaching and off-road activities prompted demographic monitoring by OPCNM starting in 1989, which continues today.

We used the database of Holm (2014), which consists of a mapped population of acuña cactus in the OPCNM. Five permanent 1000 m^2 plots were surveyed from 1991 to 2013, where all individuals, including seedlings, were marked, and their survival, volume (mm^3), and reproductive output were recorded annually. Plant volume was approximated as a cylinder using the formula $\pi\omega^2 h/4$, with height (h) and the mean of two stem widths (ω). The logarithm of the cubic root of the approximated volume was used as a state variable. In this case, the kernel in Eq. (5) was modified to include a constant q in the reproduction subkernel, which represents the probability that a seed germinates and establishes, reaching a volume $\geq$ 120 mm^3. To account for spatiotemporal differences, intercept and the slope associated with focal individual size random effects for plot (u_P) and year (u_Y) were added to equations 8. The population dynamics in relation to future climate change was investigated by Larios et al. (2020), who developed an IPM without the

consideration of intraspecific competition or any form of density dependence.

2.5. Development of the SSIIPM

Given the complexity of the SSIIPM, we built it in stages. First, we developed an aggregated model to estimate the posterior distributions of parameters for all vital rates and the interaction kernel (Eqs. (6) and 7). Next, we constructed an SSIIPM, where parameters related to the crowding effect (η and ψ in Eq. (6)) were fixed to the medians of the posterior distributions from the aggregated model. The vital rates' parameters and the population-level parameters had weak priors. N_0 used the mean observed population size in 1991, and for $\boldsymbol{\alpha}_0$, we had to set as its priors the intercepts which correspond to the relative size frequencies averaged over all plots observed in the first study year (Supplementary Material II). We opted to fix the interaction kernel's parameters of the crowding effect due to no convergence problem.

We developed the SSIIPM with the programming language Stan (Stan Development Team, 2023) and implemented it in the R environment (R Core Team, 2024) using the rstan package (Guo et al., 2024). We report the median and 89% credible interval (CI) associated with the model parameters of the crowding effect, the vital rates and the population properties, following McElreath (2020).

3. Results

3.1. Computation of the crowding effect

The crowding effect estimated for the acuña cactus population ranged from 0 to 7 units, with most individuals exhibiting values around values greater than 4. Individuals with values above one were found in clusters, suggesting that crowding impacts are significant within a 5 cm radius (Fig. 1). Due to W shape (Supplementary Material III), crowding depends more on distance and their neighbor size. Beyond 5 cm, neighbors, regardless of size or number, have negligible effects on the focal individual. A crowding effect of zero is defined when no neighbors are within 5 cm. Most individuals with significant crowding had one to three neighbors, with the nearest neighbor's size heavily influencing magnitude of the effect.

3.2. Role of individual size and crowding effect on vital rates

In the surveyed acuña cactus population, individual size was the main factor explaining vital rate differences (Table 1; Supplementary Material IV). Size had a strong positive effect on survival probability (β_1 = 0.23, 89% CI: 0.13, 0.32; Fig. 2A), with larger individuals consistently showing higher survival across the observed size range. Size was also the main driver of individual growth ($\beta_1 = 0.91$, 89% CI: 0.88, 0.94; Fig. 2C), reflected in the near 1:1 relationship between size at time t and size at $t + 1$, indicating that larger individuals largely maintain their relative size over time. Notably, focal individual size had a negligible effect on the change of crowding (β_1 = 0.014, 89% CI: −0.003, 0.033), as the credible interval spans zero, suggesting that the size of the focal individual does not strongly influence how crowded its surroundings become over time. Reproduction probability increased sharply with size ($\beta_1 = 1.42$, 89% CI: 1.30, 1.55; Fig. 2E). Similarly, the number of descendants increased with size (β_1 = 0.63, 89% CI: 0.48, 0.79; Fig. 2G), consistent with larger individuals contributing disproportionately to population recruitment.

The crowding effect (w) had contrasting effects across vital rates. Its effect on survival probability was negligible (β_2 = −0.004, 89% CI: −0.07, 0.06; Fig. 2B). However, the observed survival proportions below 0.5 at high crowding corresponded to individuals far from the median size (light points in Fig. 2B), indicating that low survival in crowded neighborhoods was concentrated in small individuals. Crowding had a clear negative effect on growth (β_2 = −0.05, 89% CI: −0.10, −0.02), so that individuals experiencing higher crowding grew less. Crowding was strongly autocorrelated through time (β_2 = 0.74, 89% CI: 0.72, 0.75; Fig. 2D), whereas focal individual size had a negligible effect on its change ($\beta_1 = 0.014$, 89% CI: −0.003, 0.033). Observed values lay close to the 1:1 line, with occasional abrupt decreases, some reaching zero, so the linear model slightly underestimated crowding at the upper end of its range. Crowding showed a positive but uncertain association with reproduction probability ($\beta_2 = 0.38$, 89% CI: −0.04, 0.74; Fig. 2F), and no detectable effect on the number of descendants ($\beta_2 = 0.04$, 89% CI: −0.05, 0.13; Fig. 2H). Finally, newborns established almost exclusively under high crowding ($w > 5$; Fig. 2J). The observed newborn distributions were multimodal for both size and crowding, which the assumed normal distributions captured only in their central tendency (Fig. 2I, J).

The random effect of the year had a variable influence on vital rates (Fig. S4). In general, random effects on the intercept showed larger

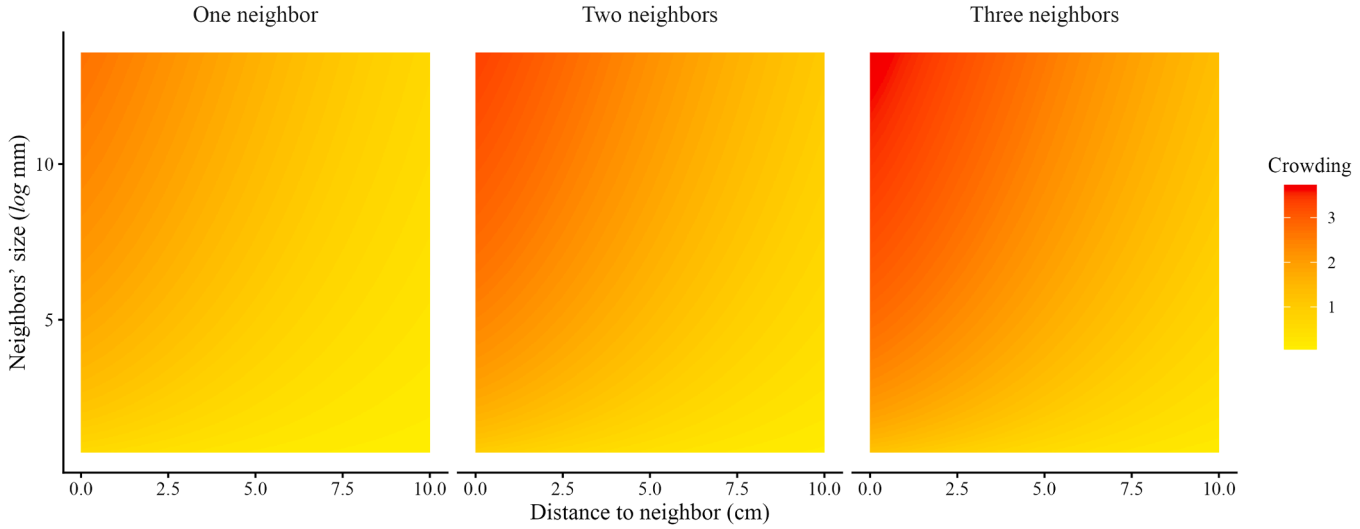

Fig. 1. Crowding effect experienced by a focal individual as a function of neighbor size, distance, and number of neighbors. The three panels correspond to scenarios with one, two, and three neighbors, respectively. Within each panel, the x-axis represents the distance from the focal individual to its neighbor(s) (cm), and the y-axis represents neighbor size (log mm). Color indicates the resulting crowding value, from low (yellow) to high (red). For simplicity, when more than one neighbor was present, all neighbors were assumed to share the same size and the same distance to the focal individual at any given point in the panel.

Table 1
Medians and 89% credible intervals (in parenthesis) for the vital rate parameter estimates for acuña cactus. Vital rate notation is described in Eq. (7).

	$s(z, w)$	$G(z', z)$	$G(w', w)$	$p(z, w)$	$f(z, w)$	$c(z')$	$c(w')$
β_0	0.37 (−0.39, 1.19)	1.46 (1.07, 1.87)	1.12 (0.80, 1.44)	−16.70 (−19.0, −14.30)	−6.03 (−7.21, −4.83)	2.80 (2.50, 3.05)	6.07 (5.65, 6.48)
β_1	0.23 (0.13, 0.32)	0.91 (0.88, 0.94)	0.014 (−0.003, 0.033)	1.42 (1.30, 1.55)	0.63 (0.48, 0.79)	—	—
β_2	−0.004 (−0.07, 0.06)	−0.05 (−0.10, −0.02)	0.74 (0.72, 0.75)	0.38 (−0.04, 0.74)	0.04 (−0.05, 0.13)	—	—
σ	—	0.44 (0.43, 0.45)	0.18 (0.17, 0.18)	—	7.40 (6.15, 9.01)	1.0 (0.91, 1.09)	0.30 (0.29, 0.32)

magnitude and more pronounced inter-annual fluctuations than random effects on the slope associated with focal individual size, indicating that most of the temporal variability in vital rates arose from shifts in baseline values rather than in size-dependence. Survival and growth in crowding showed the clearest patterns, including a marked decline in survival around 1996 and 2004, and a pronounced negative anomaly in crowding change around 2008. In contrast, reproduction probability and fecundity showed more irregular, non-directional fluctuations across years, with credible intervals for their slopes largely overlapping zero, suggesting no strong systematic effect of year on how size influenced these vital rates. Plot identity had a comparatively minor influence on vital rates (Fig. S5). Across nearly all vital rates and both intercepts and slopes, credible intervals for plot-level random effects overlapped zero, indicating no strong systematic differences among plots. The median crowding effect in the population was close to the upper end of the observed range, indicating that most individuals in the population were growing under relatively crowded conditions rather than in isolation.

3.3. Population-level estimates and SSIIPM implementation

The SSIIPM captured the overall declining trend in population size over the study period (Fig. 3), with estimated values closely tracking the observed median throughout most of the time series. However, during the early years, the model slightly overestimated total population size relative to the observed median, consistent with the plot-level overestimation seen for plots 3 and 5 during this period (Fig. S7A), which was only partially offset by a strong underestimation in plot 1. A second, more sustained period of overestimation occurred between approximately 2003 and 2007, when the estimated population size remained above the observed median (Fig. 3); this period coincides with widespread errors across most plots in Fig. S7A, indicating a general tendency of the model to overestimate population size during the population's steepest decline phase. Despite these localized discrepancies, the model successfully reproduced the overall magnitude and timing of the population decline, with estimated and observed values converging closely by the end of the study period.

The posterior distribution of the initial population size (N_0) did not include the observed mean across the five study plots ($N_{0,obs} = 57.8$ individuals; $N_{0,est} = 70.14$ individuals, 89% CI: 63.41, 77.72; Fig. S6A), indicating that the model overestimated this parameter. The estimated initial population structure was broadly consistent with the observed mean structure for both state variables, although the model overestimated the proportion of individuals in the upper size bins (Fig. 4A). The SSIIPM-projected population structures diverged from the observed mean values for both state variables over the course of the study, with the largest discrepancies occurring around the middle of the time series (e.g., 2000; Fig. 4E, F) rather than declining steadily, before converging closely with observed values by the final survey year (2013; Fig. 4G, H; Fig. S7 B).

4. Discussion

In our study, the crowding effect experienced by an individual was more dependent on the distance to its neighbors than on their number and sizes. The distance at which the neighbors have an effect on the vital rates of a focal individual was relatively small, 5 cm; individuals beyond this distance translate into little to no crowding effect. The crowding experienced by a focal individual had a clear negative effect only on its growth, whereas its effects on survival and fecundity were negligible, and its association with reproduction probability was positive but uncertain. Also, the SSIIPM correctly predicted the tendency of the population to decrease, meaning that the model captures the overall dynamics of this population.

4.1. The effect of crowding on the vital rates of E. erectocentrus

In the *E. erectocentrus* population, w had a clear negative effect on individual growth, but its effects on survival, reproduction probability, and the number of descendants were either negligible or too uncertain to distinguish from zero. This pattern is broadly compatible with demographic buffering theory, which posits that vital rates most important for population growth should be the least sensitive to environmental variation (Gaillard et al., 2000; Hilde et al., 2020; Pfister, 1998). In cacti, survival is typically the vital rate contributing most to population growth (Godínez–Álvarez et al., 2003; Jiménez-Guzmán et al., 2024; Larios et al., 2020), which may explain why crowding had little to no detectable effect on survival despite affecting growth. Because growth generally contributes less to population growth rate than survival in long-lived cacti, the population-level consequences of crowding on individual growth may be limited, potentially explaining why w had little to no effect on this cactus' overall population dynamics.

Although the credible interval for the effect of crowding on reproduction probability included the zero, the estimated trend suggested a slight increase in reproduction probability with crowding (Fig. 2F). *E. erectocentrus* var. *acunensis* is self-incompatible and pollinated primarily by solitary, polylectic bee species (Johnson, 1992), meaning that successful reproduction depends on pollinator visitation and, ultimately, on the availability of compatible mates nearby. Flower and plant density are known to influence pollinator visitation rates in a range of systems, including arid-land shrub and cactus communities, where individuals surrounded by a greater density of blooming neighbors can experience higher pollinator visitation and greater access to potential mates, a pattern generally described as pollinator-mediated facilitation (Hurtado et al., 2023). If a similar mechanism operates in the acuña cactus, individuals growing in denser conspecific neighborhoods could benefit from increased pollinator activity or a larger local pool of compatible mates, potentially offsetting the negative effect of crowding on growth. However, given the wide credible interval around this estimate, this potential facilitation effect remains speculative and would require direct observations of pollinator visitation rates across a gradient of crowding to be confirmed.

Contrary to expectations for a species assumed to grow largely in isolation, the observed median crowding effect value in the population was relatively high ($w \approx 6$), close to the upper end of the observed range, indicating that most focal individuals were growing under substantial crowding rather than in isolation (Larios et al., 2020). New individuals often establish near their parent plants, which may explain the prevalence of moderate to high crowding values in the population, while occasional isolated individuals may arise from animal-dispersed seeds or the natural isolation of surviving descendants. Similarly, abrupt changes in crowding between time t and $t + 1$ (Fig. 2D) likely reflect the death of neighbors associated with the focal plant. These processes may explain the bimodal distribution of crowding values observed in Fig. 2J,

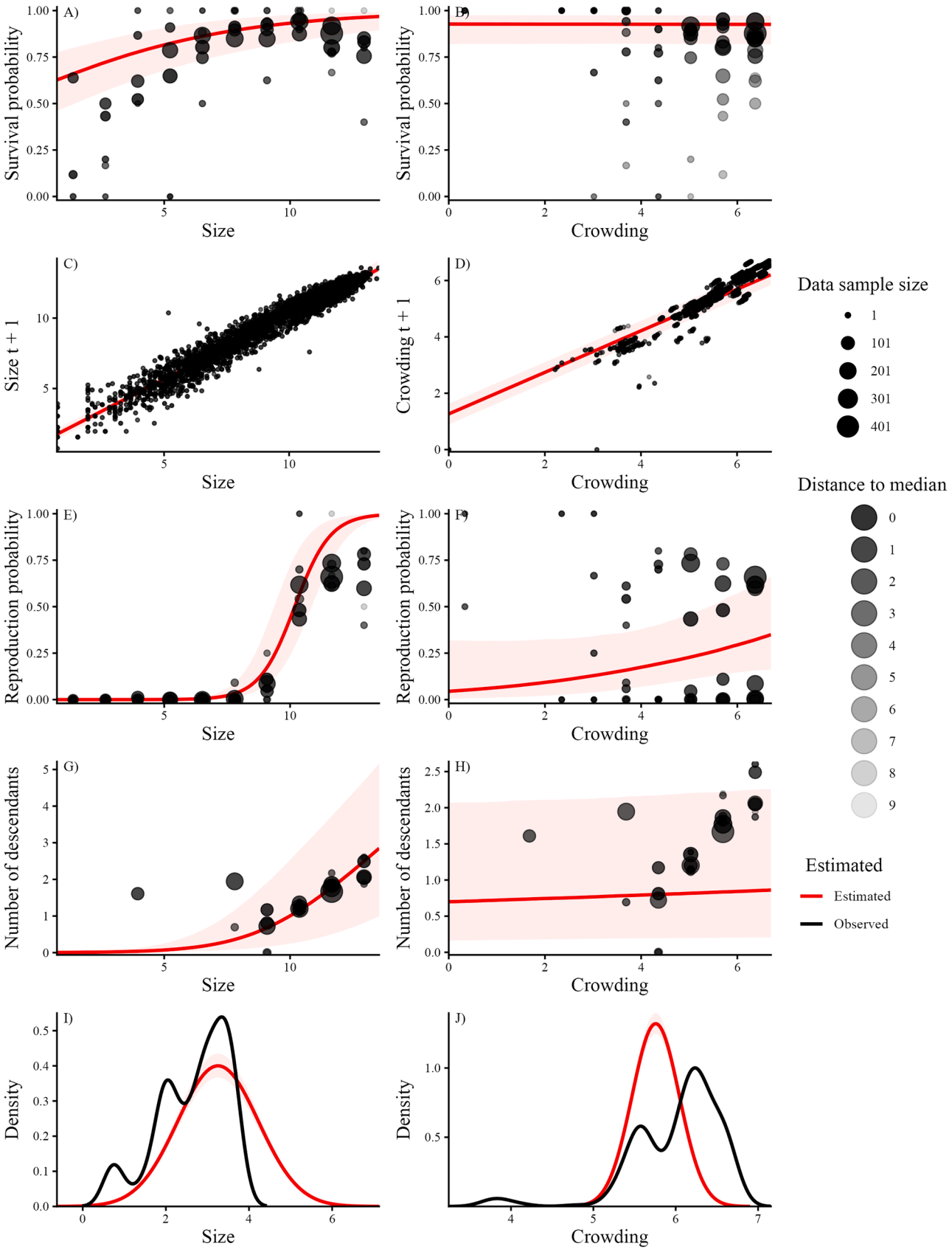

(caption on next page)

Fig. 2. Vital rates estimated using the Spatially Structured Integrated Integral Population Model (SSIIPM). Left column: vital rates as functions of size at the median crowding effect ($w \approx 6$); right column: vital rates as functions of crowding effect at the median size ($z = 9.89$). **A** & **B)** Survival probability, **C)** Growth in size, **D)** Change in crowding effect, **E** & **F)** Reproduction probability, **G** & **H)** Logarithm of the number of descendants, **I** & **J)** Size and crowding effect distributions of newborns. Red lines represent posterior medians of the estimated vital rates, excluding plot and year random effects, and light red areas their 89% credible intervals. Points represent observed data. In **C** & **D**, points are individual observations. In **A, B, E, F, G** & **H**, data were grouped into the cells of the discretized size × crowding grid, and points represent the proportion of individuals that survived or reproduced (**A, B, E** & **F**) or the mean number of descendants (**G** & **H**) within each cell. Cells of all classes of the other state variable are shown, with point size indicating the number of individuals in the cell and point shading indicating the distance of its class to the median class (darker = closer). Because the estimated curve is evaluated only at the median, points from classes far from the median are not expected to lie on it.

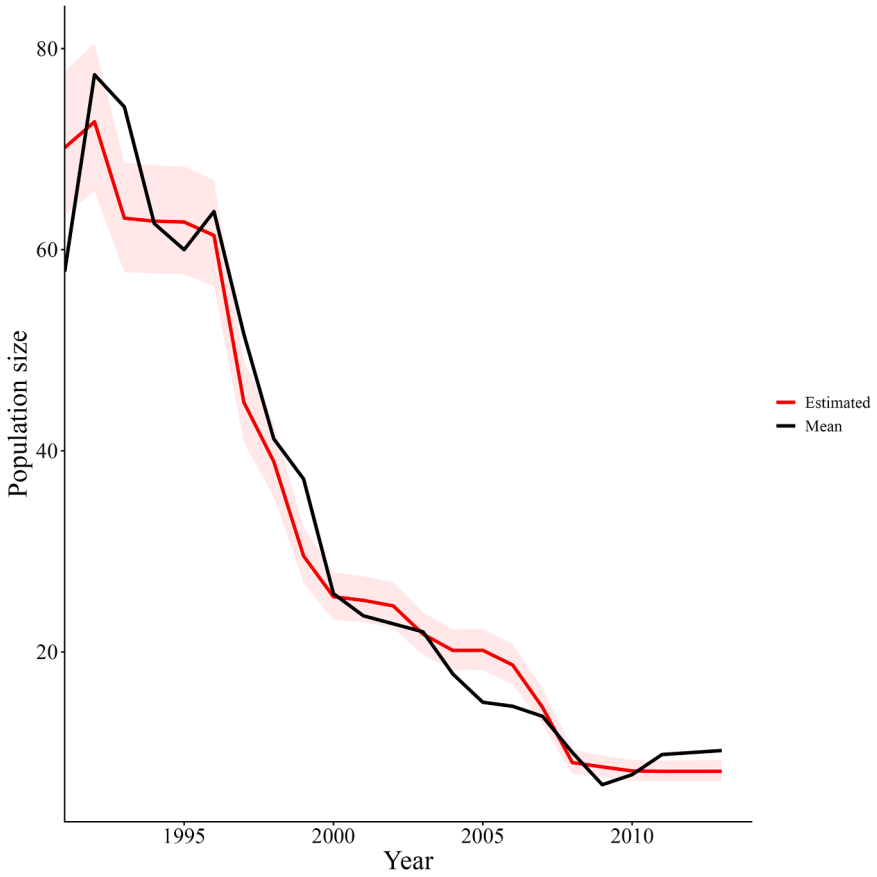

Fig. 3. Observed (black) and estimated (red) population size across the study period (1991–2013). The black line shows the mean population size across the five monitored plots, and the red line shows the model-estimated population size, with the shaded band representing its 89% credible interval.

reflecting the co-existence of isolated and highly crowded individuals within the population.

Some discrepancies between observed and estimated vital rates point to possible model refinements. The model overestimated survival of the smallest individuals (Fig. 2A) and reproduction probability of the largest ones (Fig. 2E). In addition, the assumed normal distributions did not capture the multimodality of newborn size and crowding (Fig. 2I, J), nor the asymmetric dynamics of crowding, which is characterized by persistence and occasional abrupt decreases (Fig. 2D). Mixture distributions for newborns and zero-inflated or asymmetric distributions for the change in crowding could improve the representation of these processes in future applications.

4.2. Population attributes and implementation of the SSIIPM

The SSIIPM successfully captured the overall population decline (Fig. 3), owing to the incorporation of population-level data, particularly for estimating establishment probability (q) in Eq. (10). This demonstrates the value of population-level data for estimating parameters that are difficult to obtain from individual-level data (González et al., 2016; Portillo-Tzompa et al., 2023), and it largely improved model predictions compared to a non-integrated version of the model that excludes population-level data (SSIPM; Fig. S8). This advantage, however, comes with a limitation. Because q is informed only by population-level data, we assumed it to be constant, which is reasonable at the local scale of this study but may not hold across larger areas with contrasting biotic and abiotic conditions. Allowing q to vary in space would require additional information on establishment, such as seedling emergence or seed addition experiments, to avoid identifiability problems.

The model overestimated the initial population size, with the 89% credible interval not encompassing the observed value. The initial population structure, in contrast, was broadly consistent with the observed mean structure for both state variables, except for an overestimation of the upper size bins (Fig. 4A). The discrepancies between estimated and observed structures did not decrease steadily but peaked around the middle of the study period, before converging by the final survey year (Fig. 4). This convergence may partly reflect the weak ergodicity of structured population models, whereby the influence of initial conditions on population structure diminishes over successive

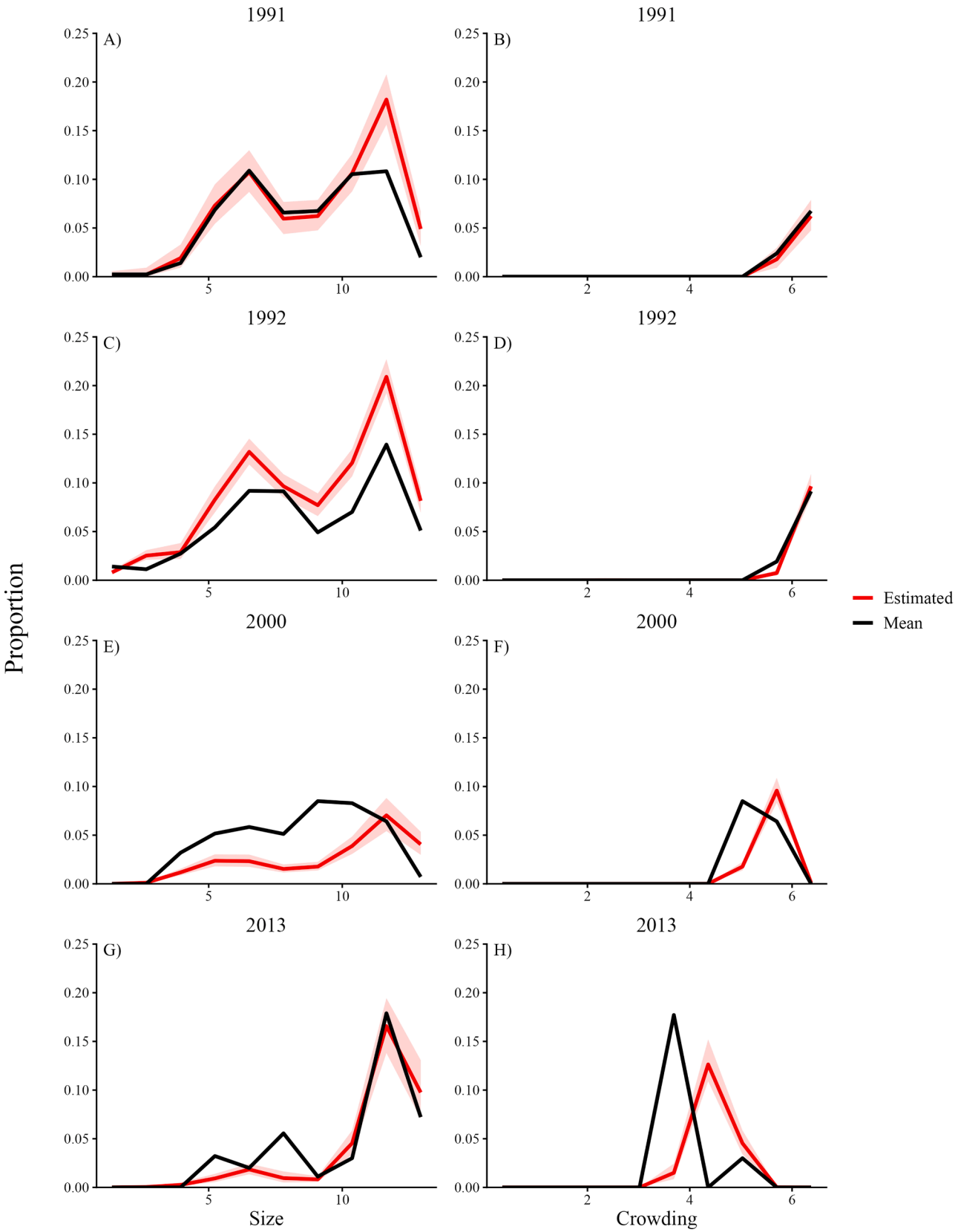

Fig. 4. Observed (black) and estimated (red) population structure in terms of size (**A, C, E, G**) and crowding effect (**B, D, F, H**) for four years of the study period (1991, 1992, 2000, and 2013). The black line shows the mean population structure and the shaded red band represents the 89% credible interval of the estimated structure. Population structures are projected at the observed median values of the other state variable.

iterations (Ellner and Rees, 2007). It may also reflect that, as population size declined toward very low values (Fig. 3), absolute differences between structures were increasingly constrained by the small number of individuals distributed across size and crowding classes (Fig. S7). Including year random effects on both the intercept and the size slope of vital rates allowed the model to capture localized periods of increase, rather than a strictly monotonic projection. Nevertheless, the model overestimated population size during the steepest phase of the decline (2003–2007; Fig. 3).

Population-level data alone do not identify the causes of the decline, but the available evidence suggests that it resulted mainly from the loss of a large cohort of young individuals, recruited during the wet years of the early 1990s (Larios et al., 2020), that was not replaced by new recruitment (U.S. Fish and Wildlife Service, 2013). This is consistent with the low survival of small individuals (Fig. 2A) and with the overestimation of population size during 2003–2007, which, given that q was assumed constant through time, suggests that establishment was even lower than average in those years. The survival decreased around 1996 (Fig. S4), which coincided with the sharpest decline in the plots, may reflect biotic factors such as small mammal predation (Larios et al., 2020; Rosen, 2000), since direct climatic effects on this population are weak (Larios et al., 2020). Crowding, in contrast, affected growth but not survival and is unlikely to have driven the decline, although its uncertain positive effect on reproduction suggests a possible Allee effect: in this self-incompatible, pollinator-dependent species (Johnson, 1992), lower densities could reduce mate availability and thus reinforce the decline.

4.3. Crowding as a dual state variable versus a population-level quantity

We conceptualize the crowding effect (w) as a dual state variable: it is a property of the focal individual, since it depends on its position, but it is also determined by its neighbors, through their presence, distance, and size. Unlike intrinsic state variables such as size, w therefore changes not only with the focal individual but also with the dynamics of its neighborhood, including neighbor growth, survival, and recruitment.

Previous models have instead represented crowding as a population-level quantity. In these models, crowding may be a single value shared by all individuals (Preuss et al., 2009; Vanoverbeke, 2008) or, alternatively, it may be a function of the focal individual's size, which implicitly assumes an average neighborhood for each size, so that all individuals of the same size experience the same crowding (Adler et al., 2010, 2012, 2018b). These approximations simplify modeling but do not necessarily capture the fact that individuals of the same size can occupy neighborhoods with very different crowding levels (Tamura et al., 2019).

Whether crowding can be represented as a population-level quantity or as a dual state variable depends on how organisms move and interact in space (Law et al., 2003). When individuals move freely and randomly, each one interacts, on average, with the same neighbors over time, so that the crowding experienced by all individuals in the population is effectively the same (Preuss et al., 2009; Vanoverbeke, 2008). Similarly, representing crowding as a function of focal individual size (Adler et al., 2010, 2012, 2018b) is adequate when individuals are randomly distributed in space and interact with many neighbors, so that differences among neighborhoods average out and individuals of the same size experience similar crowding. In sessile organisms with local interactions and aggregated distributions, neither condition holds (Pacala and Silander, 1985). In the acuña cactus, crowding was restricted and most individuals had only one to three neighbors within the radius in which crowding was significant. Moreover, crowding was strongly autocorrelated through time ($\beta_2 = 0.74$), so an individual's crowding is a persistent individual attribute rather than a transient population-wide condition. The SSIIPM captures this by structuring the population independently by size and crowding and by including a transition function for crowding, $G(w', w)$. Despite these differences, all these approaches agree that conspecific density dependence should be incorporated for population models to better reproduce observed dynamics.

This added realism comes at a cost, parameters η and ζ, defining the interaction kernel's shape and scale, must be estimated alongside vital rates since direct measurements of this kernel are not feasible. The estimated w values are also used to construct w_k-bins, requiring an integrated estimation of interaction kernel parameters, vital rates, and population-level parameters through computationally intensive methods.

4.4. Advances, broader applicability, and implications for good modeling practice

The SSIIPM advances current approaches to modeling crowding in three ways. First, crowding is treated as a dynamic dual state variable in the kernel, rather than as a function of focal individual size (Adler et al., 2010, 2012; Teller et al., 2016) or as a population-level quantity shared by all individuals (Preuss et al., 2009; Vanoverbeke, 2008). Second, the spatial scale and shape of the interaction are estimated from the data rather than fixed a priori, and crowding is allowed to affect all vital rates, including reproduction. Third, the spatial structure is combined with population-level data within a Bayesian framework, which allows the estimation of processes for which no individual-level data exist, such as establishment probability. For the acuña cactus, this represents, to our knowledge, the first demographic analysis to incorporate density dependence (cf. Larios et al., 2020). It shows that crowding reduces growth without detectably affecting survival, and that the population comprises both isolated and strongly aggregated individuals, information relevant to the spatial design of reintroductions of this endangered species.

Despite its added complexity, incorporating crowding as a state variable provided insights that would be missed by other approaches. Because w reflects both the spatial distribution of individuals and their intraspecific interactions, it allows identifying which vital rates respond to aggregation and in which direction. In addition, representing population structure in terms of w provides more information than summary indices of spatial pattern such as Ripley's K (Baddeley et al., 2015), revealing, for instance, the bimodal distribution of crowding in the acuña cactus population, where isolated and strongly aggregated individuals coexist.

Although we illustrated the framework with a sessile plant, it applies to any system where individuals interact locally and their positions are recorded. Examples include permanent forest plots, sessile marine invertebrates such as corals and mussels, colonial or territorial animals, and spreading invasive plants. Beyond population ecology, the same structure, an individual exposure computed through a distance-weighted kernel and tracked over time, is relevant to agronomy and forestry (planting density, intercropping, thinning), and restoration planting design.

Our work also offers more general lessons for good modeling practice. First, whether interactions are represented through averages or through a spatially explicit representation is a modeling decision that should be stated and justified, not assumed by default. We suggest that the relative scales of organism movement and interaction serve as an explicit criterion for this choice. Average crowding is appropriate for well-mixed vagile organisms, whereas sessile organisms with interaction ranges much smaller than the study area require explicit neighborhoods; this illustrates the transparent justification of scale choices identified by Jakeman et al. (2024). Second, integrating individual- and population-level data offers a route to estimate otherwise unobservable processes, contributing to robust parameterization frameworks. Third, analyses such as ours are only possible when demographic monitoring programs record the positions of individuals, an inexpensive addition that should be considered when planning data acquisition.

5. Conclusions

We developed the Spatially Structured Integrated Integral Population Model (SSIIPM), incorporating the crowding effect as a state variable to assess the impact of intraspecific interactions on individual performance and population dynamics. This approach demonstrated the value of integrating population-level information to enhance predictions, as models without this integration deviated significantly from observed data. In the acuña cactus, crowding reduced growth but had no detectable effect on survival or fecundity, and a positive but uncertain association with reproduction, suggesting that spatial aggregation has differential effects on vital rates. By including the crowding effect, the model successfully accounts for the heterogeneous spatial distribution of individuals on the dynamics of a population.

Funding

This work was supported by a scholarship granted to IR-G by the Consejo Nacional de Humanidades, Ciencias y Tecnologías (CONAHCYT) / Secretaría de Ciencia, Humanidades, Tecnología e Innovación (SECIHTI).

Declaration of generative AI and AI-assisted technologies in the writing process

During the preparation of this work the author(s) used Claude (Anthropic) in order to improve the language and readability of the manuscript. After using this tool, the authors reviewed and edited the content as needed and take full responsibility for the content of the publication.

CRediT authorship contribution statement

Iván Romero-García: Writing – review & editing, Writing – original draft, Methodology, Formal analysis, Conceptualization. **Eugenio Larios:** Writing – review & editing, Resources. **Edgar J. González:** Writing – review & editing, Supervision, Methodology, Conceptualization.

Declaration of competing interest

The authors declare that they have no known competing financial interests or personal relationships that could have appeared to influence the work reported in this paper.

Acknowledgements

This paper serves as a fulfillment of IR-G to obtain his M.Sc. (Ecology) degree in the Posgrado en Ciencias Biológicas, UNAM. We thank Phillip C. Rosen, Amie Pate, and Pete Holm for providing the data used in this study. We thank Paola I. Portillo-Tzompa for her support in the construction of the integrated part of the model. Finally, we thank Ernesto V. Vega-Peña and Carlos Díaz-Avalos for their insightful comments during the model development process.

Supplementary materials

Supplementary material associated with this article can be found, in the online version, at doi:10.1016/j.ecolmodel.2026.111932.

Data availability

Data will be made available on request.

References

Adler, P.B., Dalgleish, H.J., Ellner, S.P., 2012. Forecasting plant community impacts of climate variability and change: when do competitive interactions matter?: climate and species interactions. J. Ecol. 100 (2), 478–487. https://doi.org/10.1111/j.1365-2745.2011.01930.x.

Adler, P.B., Ellner, S.P., Levine, J.M., 2010. Coexistence of perennial plants: an embarrassment of niches. Ecol. Lett. 13 (8), 1019–1029. https://doi.org/10.1111/j.1461-0248.2010.01496.x.

Adler, P.B., Kleinhesselink, A., Hooker, G., Taylor, J.B., Teller, B., Ellner, S.P., 2018b. Weak interspecific interactions in a sagebrush steppe? Conflicting evidence from observations and experiments. Ecology 99 (7), 1621–1632. https://doi.org/10.1002/ecy.2363.

Adler, P.B., Smull, D., Beard, K.H., Choi, R.T., Furniss, T., Kulmatiski, A., Meiners, J.M., Tredennick, A.T., Veblen, K.E., 2018a. Competition and coexistence in plant communities: intraspecific competition is stronger than interspecific competition. Ecol. Lett. 21 (9), 1319–1329. https://doi.org/10.1111/ele.13098.

Aranda-Pineda, J.A., Valverde, P.L., Búrquez, A., Golubov, J., Mandujano, M.C., 2021. Effect of brousse tigrée on the dynamics of nurse–protégé interactions of a cactus in the Chihuahuan Desert. Plant Species Biol. 36, 450–462. https://doi.org/10.1111/1442-1984.12329.

Armas, C., Pugnaire, F.I., 2009. Ontogenetic shifts in interactions of two dominant shrub species in a semi-arid coastal sand dune system. J. Veg. Sci. 20 (3), 535–546. https://doi.org/10.1111/j.1654-1103.2009.01055.x.

Baddeley, A., Rubak, E., Turner, R., 2015. Spatial Point Patterns: Methodology and Applications with R. Chapman & Hall/CRC.

Barber, C., Zaiats, A., Applestein, C., Rosenthal, L., Caughlin, T.T., 2022. Bayesian models for spatially explicit interactions between neighbouring plants. Methods Ecol. Evol. 13 (12), 2788–2798. https://doi.org/10.1111/2041-210X.13998.

Callaway, R.M., Walker, L.R., 1997. Competition and facilitation: a synthetic approach to interactions in plant communities. Ecology 78 (7), 1958. https://doi.org/10.2307/2265936.

Crone, E.E., 2016. Contrasting effects of spatial heterogeneity and environmental stochasticity on population dynamics of a perennial wildflower. J. Ecol. 104 (2), 281–291. https://doi.org/10.1111/1365-2745.12500.

Dahlgren, J.P., Ehrlén, J., 2009. Linking environmental variation to population dynamics of a forest herb. J. Ecol. 97 (4), 666–674. https://doi.org/10.1111/j.1365-2745.2009.01504.x.

Doak, D.F., Waddle, E., Langendorf, R.E., Louthan, A.M., Isabelle Chardon, N., Dibner, R., Keinath, D.A., Lombardi, E., Steenbock, C., Shriver, R.K., Linares, C., Begoña Garcia, M., Funk, W.C., Fitzpatrick, S.W., Morris, W.F., DeMarche, M.L., 2021. A critical comparison of integral projection and matrix projection models for demographic analysis. Ecol. Monogr. 91 (2), e01447. https://doi.org/10.1002/ecm.1447.

Dunning, J.B., Stewart, D.J., Danielson, B.J., Noon, B.R., Root, T.L., Lamberson, R.H., Stevens, E.E., 1995. Spatially explicit population models: current forms and future uses. Ecol. Appl. 5 (1), 3–11. https://doi.org/10.2307/1942045.

Ellner, S.P., Childs, D.Z., Rees, M., 2016. Data-driven Modelling of Structured Populations: A Practical Guide to the Integral Projection Model. Springer International Publishing. https://doi.org/10.1007/978-3-319-28893-2.

Ellner, S.P., Rees, M., 2007. Stochastic stable population growth in integral projection models: theory and application. J. Math. Biol. 54 (2), 227–256. https://doi.org/10.1007/s00285-006-0044-8.

Gaillard, J.-M., Festa-Bianchet, M., Yoccoz, N.G., Loison, A., Toïgo, C., 2000. Temporal variation in fitness components and population dynamics of large herbivores. Annu Rev. Ecol. Syst. 31 (1), 367–393. https://doi.org/10.1146/annurev.ecolsys.31.1.367.

Ghosh, S., Gelfand, A.E., Clark, J.S., 2012. Inference for size demography from point pattern data using integral projection models. J. Agric. Biol. Environ. Stat. 17 (4), 641–677. https://doi.org/10.1007/s13253-012-0123-9.

Godínez–Álvarez, H., Valverde, T., Ortega–Baes, P., 2003. Demographic trends in the Cactaceae. Bot. Rev. 69 (2), 173–203. https://doi.org/10.1663/0006-8101(2003)069[0173:DTITC]2.0.CO;2.

González, E.J., Martorell, C., Bolker, B.M., 2016. Inverse estimation of integral projection model parameters using time series of population-level data. Methods Ecol. Evol. 7 (2), 147–156. https://doi.org/10.1111/2041-210X.12519.

Gu, M., Zhang, Y., Wen, Y., Ai, G., Zhang, H., Wang, P., Wang, G., 2023. A lightweight convolutional neural network hardware implementation for wearable heart rate anomaly detection. Comput. Biol. Med. 155, 106623. https://doi.org/10.1016/j.compbiomed.2023.106623.

Guo, J., Gabry, J., Goodrich, B., Johnson, A., Weber, S., Badr, H.S., 2024. RSTAN: r Interface to Stan. https://mc-stan.org/rstan/.

Haefner, J.W., Poole, G.C., Dunn, P.V., Decker, R.T., 1991. Edge effects in computer models of spatial competition. Ecol. Model. 56, 221–244. https://doi.org/10.1016/0304-3800(91)90201-B.

Hamrick, J.L., Lee, J.M., 1987. Effect of soil surface topography and litter cover on the germination, survival, and growth of musk thistle (*Carduus nutans*). Am. J. Bot. 74 (3), 451–457. https://doi.org/10.1002/j.1537-2197.1987.tb08627.x.

Hara, T., 1988. Dynamics of size structure in plant populations. Trends. Ecol. Evol. 3 (6), 129–133. https://doi.org/10.1016/0169-5347(88)90175-9.

Hilde, C.H., Gamelon, M., Sæther, B.-E., Gaillard, J.-M., Yoccoz, N.G., Pélabon, C., 2020. The demographic buffering hypothesis: evidence and challenges. Trends. Ecol. Evol. 35 (6), 523–538. https://doi.org/10.1016/j.tree.2020.02.004.

P. Holm (2014). Chapter 2: Acuna Cactus. In: organ Pipe Cactus National Monument. ORPI Ecol. Monit. Program Rep. https://www.nps.gov/orpi/learn/nature/orpi-ecological-monitoring-report.htm.

Hurtado, M., Godoy, O., Bartomeus, I., 2023. Plant spatial aggregation modulates the interplay between plant competition and pollinator attraction with contrasting outcomes of plant fitness. Web. Ecol. 23 (1), 51–69. https://doi.org/10.5194/we-23-51-2023.

Hutchings, M.J., John, E.A., Wijesinghe, D.K., 2003. Toward understanding the consequences of soil heterogeneity for plant populations and communities. Ecology 84 (9), 2322–2334. https://doi.org/10.1890/02-0290.

Jakeman, A.J., Elsawah, S., Wang, H.-H., Hamilton, S.H., Melsen, L., Grimm, V., 2024. Towards normalizing good practice across the whole modeling cycle: its instrumentation and future research topics. Socio.-Environ. Syst. Model. 6, 18755. https://doi.org/10.18174/sesmo.18755.

Jia, X., Zhang, W.-P., 2026. Shoot facilitation contributes more than root facilitation to plant size inequality under environmental stress: theoretical insights from a two-layer zone-of-influence model. Plant Soil 523, 61–74. https://doi.org/10.1007/s11104-024-07056-0.

Jiménez-Guzmán, G., Arroyo-Cosultchi, G., Martorell, C., Martínez-Ramos, M., Vega-Peña, E.V., 2024. What do we know about the demographic modeling of cacti? A systematic review of current knowledge. J. Arid. Environ. 224, 105226. https://doi.org/10.1016/j.jaridenv.2024.105226.

Johnson, R.A., 1992. Pollination and reproductive ecology of Acuña Cactus, *echinomastus erectrocentrus* var. *Acunensis* (Cactaceae). Int. J. Plant Sci. 153 (3, Part 1), 400–408. https://doi.org/10.1086/297044.

Larios, E., González, E.J., Rosen, P.C., Pate, A., Holm, P., 2020. Population projections of an endangered cactus suggest little impact of climate change. Oecologia 192 (2), 439–448. https://doi.org/10.1007/s00442-020-04595-y.

Law, R., Murrell, D.J., Dieckmann, U., 2003. Population growth in space and time: spatial logistic equations. Ecology 84 (1), 252–262. https://doi.org/10.1890/0012-9658(2003)084[0252:PGISAT]2.0.CO;2.

Lin, Y., Berger, U., Grimm, V., Ji, Q., 2012. Differences between symmetric and asymmetric facilitation matter: exploring the interplay between modes of positive and negative plant interactions. J. Ecol. 100 (6), 1482–1491. https://doi.org/10.1111/j.1365-2745.2012.02019.x.

Lyu, S., Alexander, J.M., 2023. Compensatory responses of vital rates attenuate impacts of competition on population growth and promote coexistence. Ecol. Lett. 26 (3), 437–447. https://doi.org/10.1111/ele.14167.

McElreath, R., 2020. Statistical Rethinking: A Bayesian Course with Examples in R and Stan, 2nd ed. Chapman and Hall/CRC. https://doi.org/10.1201/9780429029608.

McIntosh, M.E., Boyd, A.E., Arnold, A.E., Steidl, R.J., McDade, L.A., 2020. Growth and demography of a declining, endangered cactus in the Sonoran Desert. Plant Species Biol. 35 (1), 6–15. https://doi.org/10.1111/1442-1984.12251.

Merow, C., Dahlgren, J.P., Metcalf, C.J.E., Childs, D.Z., Evans, M.E.K., Jongejans, E., Record, S., Rees, M., Salguero-Gómez, R., McMahon, S.M., 2014a. Advancing population ecology with integral projection models: a practical guide. Methods Ecol. Evol. 5 (2), 99–110. https://doi.org/10.1111/2041-210X.12146.

Merow, C., Latimer, A.M., Wilson, A.M., McMahon, S.M., Rebelo, A.G., Silander, J.A., 2014b. On using integral projection models to generate demographically driven predictions of species' distributions: development and validation using sparse data. Ecography 37 (12), 1167–1183. https://doi.org/10.1111/ecog.00839.

Metz, J.A.J., 2008. Fitness. In: Sven Erik, J., Fath, B.D. (Eds.), Encyclopedia of Ecology. Academic Press, pp. 1599–1612.

Miriti, M.N., 2006. Ontogenetic shift from facilitation to competition in a desert shrub. J. Ecol. 94 (5), 973–979. https://doi.org/10.1111/j.1365-2745.2006.01138.x.

Pacala, S.W., 1987. Neighborhood models of plant population dynamics 3. Models with spatial heterogeneity in the physical environment. Theor. Popul. Biol. 31 (3), 359–392. https://doi.org/10.1016/0040-5809(87)90012-8.

Pacala, S.W., Silander, J.A., 1985. Neighborhood models of plant population dynamics. I. Single-species models of annuals. Am. Nat. 125 (3), 385–411. https://doi.org/10.1086/284349.

Pfister, C.A., 1998. Patterns of variance in stage-structured populations: evolutionary predictions and ecological implications. Proc. Natl. Acad. Sci. 95 (1), 213–218. https://doi.org/10.1073/pnas.95.1.213.

Portillo-Tzompa, P., Martín-Cornejo, P.R., González, E.J., 2023. Integrated integral population models. bioRxiv. https://doi.org/10.1101/2023.10.24.563870, 2023.10.24.563870bioRxiv.

Preuss, T.G., Hammers-Wirtz, M., Hommen, U., Rubach, M.N., Ratte, H.T., 2009. Development and validation of an individual based *Daphnia magna* population model: the influence of crowding on population dynamics. Ecol. Model. 220 (3), 310–329. https://doi.org/10.1016/j.ecolmodel.2008.09.018.

R Core Team, 2024. R: a language and environment for statistical computing. R. Found Stat. Comput. https://www.R-project.org/.

Rees, M., Childs, D.Z., Ellner, S.P., 2014. Building integral projection models: a user's guide. J. Anim. Ecol. 83 (3), 528–545. https://doi.org/10.1111/1365-2656.12178.

Ren, J., Wang, H., 2023. Calculus and optimization. Mathematical Methods in Data Science. Elsevier, pp. 51–89. https://doi.org/10.1016/B978-0-44-318679-0.00009-0.

Rosen, P.C., 2000. *A monitoring study of vertebrate community ecology in the northern Sonoran Desert, Arizona* [Doctoral dissertation, University of Arizona]. http://hdl.handle.net/10150/289117.

Sanczuk, P., De Pauw, K., De Lombaerde, E., Luoto, M., Meeussen, C., Govaert, S., Vanneste, T., Depauw, L., Brunet, J., Cousins, S.A.O., Gasperini, C., Hedwall, P.-O., Iacopetti, G., Lenoir, J., Plue, J., Selvi, F., Spicher, F., Uria-Diez, J., Verheyen, K., De Frenne, P., 2023. Microclimate and forest density drive plant population dynamics under climate change. Nat. Clim. Change 13 (8), 840–847. https://doi.org/10.1038/s41558-023-01744-y.

Scanga, S.E., 2014. Population dynamics in canopy gaps: nonlinear response to variable light regimes by an understory plant. Plant Ecol. 215 (8), 927–935. https://doi.org/10.1007/s11258-014-0344-9.

Schwinning, S., Weiner, J., 1998. Mechanisms determining the degree of size asymmetry in competition among plants. Oecologia 113 (4), 447–455. https://doi.org/10.1007/s004420050397.

Stan Development Team, 2023. Stan Modeling Language User's Guide and Reference Manual, version 2.32. https://mc-stan.org/docs/2_32/reference-manual/index.html.

Tamura, M., Ohgushi, T., Ida, T.Y., 2020. Intraspecific neighbourhood effect: population-level consequence of aggregation of highly defended plants. Funct. Ecol. 34, 597–605. https://doi.org/10.1111/1365-2435.13515.

Teller, B.J., Adler, P.B., Edwards, C.B., Hooker, G., Ellner, S.P., 2016. Linking demography with drivers: climate and competition. Methods Ecol. Evol. 7 (2), 171–183. https://doi.org/10.1111/2041-210X.12486.

Tyler, C.M., D' Antonio, C.M., 1995. The effects of neighbors on the growth and survival of shrub seedlings following fire. Oecologia 102 (2), 255–264. https://doi.org/10.1007/BF00333258.

U.S. Fish and Wildlife Service, Interior, 2013. Endangered and threatened wildlife and plants; endangered species status for *echinomastus erectocentrus* var. *Acunensis* (Acuña cactus) and *pediocactus peeblesianus* var. *Fickeiseniae* (Fickeisen plains cactus) throughout their ranges. Fed. Regist. 78 (190), 60608–60652.

Vanoverbeke, J., 2008. Modeling individual and population dynamics in a consumer–resource system: behavior under food limitation and crowding and the effect on population cycling in *Daphnia*. Ecol. Model. 216 (3–4), 385–401. https://doi.org/10.1016/j.ecolmodel.2008.05.009.

Williams, J.L., Miller, T.E.X., Ellner, S.P., 2012. Avoiding unintentional eviction from integral projection models. Ecology 93 (9), 2008–2014. https://doi.org/10.1890/11-2147.1.

Zhang, L., Gao, Y., Li, J., Zhang, C., Li, M., Hu, Z., Cui, X., 2022. Effects of grazing disturbance of spatial distribution pattern and interspecies relationship of two desert shrubs. J. For. Res. 33 (2), 507–518. https://doi.org/10.1007/s11676-021-01353-5.